Potassium channel receptor site for the inactivation gate and quaternary amine inhibitors

Ming Zhou, João H. Morais-Cabral*, Sabine Mann & Roderick MacKinnon

Howard Hughes Medical Institute, Laboratory of Molecular Neurobiology and Biophysics, Rockefeller University, 1230 York Avenue, New York, New York 10021, USA

Many voltage-dependent K^+ channels open when the membrane is depolarized and then rapidly close by a process called inactivation. Neurons use inactivating K^+ channels to modulate their firing frequency. In Shaker-type K^+ channels, the inactivation gate, which is responsible for the closing of the channel, is formed by the channel's cytoplasmic amino terminus. Here we show that the central cavity and inner pore of the K^+ channel form the receptor site for both the inactivation gate and small-molecule inhibitors. We propose that inactivation occurs by a sequential reaction in which the gate binds initially to the cytoplasmic channel surface and then enters the pore as an extended peptide. This mechanism accounts for the functional properties of K^+ channel inactivation and indicates that the cavity may be the site of action for certain drugs that alter cation channel function.

The presence of an inactivation gate causes a K^+ channel to close spontaneously after opening induced by membrane depolarization (Fig. 1a). The inactivation gate in Shaker-type K^+ channels is formed by the first 20 amino acids on the N terminus of the α-subunit[1,2] or β-subunit[3], located on the intracellular side of the membrane (Fig. 1c, d). The essential chemical characteristics that enable the N terminus to act as a gate are that the first approximately 10 amino acids tend to be hydrophobic (hydrophobic region) and the remaining 10 hydrophilic with excess positive charge (hydrophilic region)[4,5] (Fig. 1d).

Four lines of evidence support the idea that the inactivation gate binds to the pore. First, inactivation occurs only after the voltage-dependent gate opens, as if the opening of the pore exposes a receptor for the gate[6]. Second, inactivation is produced by the binding of only one gate, presumably to the single pore opening, even though K^+ channels have four gates (N termini), by virtue of their homotetrameric architecture[7,8]. Third, high concentrations of extracellular K^+ reduce inactivation, as if K^+ ions traversing the pore push the gate from its intracellular site[9]. Fourth, inactivation mimics the action of quaternary amines, which are thought to be pore blockers[10,11] (Fig. 1a, b). Furthermore, quaternary amines compete with the gate to inhibit K^+ current[11].

How does the N-terminal gate interact with the pore to cause inactivation? Studies using mutagenesis have highlighted amino acids that might be expected to reside near the intracellular pore opening, for example, those between the fourth and fifth membrane-spanning segments, which connect the voltage sensor to the pore module[12]. In addition, the structures of inactivation gates have been analysed by NMR spectroscopy[13,14]. Together, these approaches have led to a picture of an inactivation 'domain' capping the pore's intracellular face[13,15]. This picture is reasonable, but the quantitative details of earlier work are more compatible with a different structural view[4,5].

Pore occlusion by an extended N terminus

Structural studies have shown that the pore of a voltage-dependent K^+ channel opens to the cytoplasm between the T1 domain and the transmembrane channel[16–18] (Fig. 1c). On the basis of mutant cycle analysis, the inactivation gate was proposed to reach its site of action by entering the openings above the T1 domain[16] (Fig. 1c). Here we ask, where is the inactivation gate's site of action? To address this question, we studied inactivation mediated by the β1 subunit inactivation gate attached to the β2 core (β12)[16,19] (Fig. 1c, d). The β12 subunit was expressed in *Xenopus* oocytes with the $K_v1.4$ channel α-subunit, a mammalian homologue of the Shaker K^+ channel. The $K_v1.4$ α-subunit contained a deletion in its own N terminus (1.4-IR; see Methods) to ensure that inactivation would be mediated only by the β12 inactivation gate[16,19] (Fig. 1a). The inactivation process was parameterized by the inactivation time constants τ_{on}, τ_{off} and the ratio τ_{on}/τ_{off}, referred to as K_d (the dissociation constant: see Fig. 2a and Methods).

Mutations to alanine or to valine (position 6) in the inactivation gate affected K_d, a measure of the apparent affinity of the gate for its receptor, in a manner very consistent with previous findings on the Shaker K^+ channel[1,2,4,5] (Fig. 2a). Mutations in the hydrophobic region had large energetic effects, expressed as changes in the apparent dissociation rate constant ($1/\tau_{off}$), whereas those in the hydrophilic region had more modest effects and altered both the apparent association ($1/\tau_{on}$) and dissociation rate constants. The importance of residues very close to the N terminus, in the hydrophobic region, is emphasized by the observation that a peptide corresponding to the first four amino acids alone (with a carboxy-terminal amide rather than a carboxylic acid) retains some ability to inhibit K^+ current (Fig. 2b).

The sixth membrane-spanning segment of voltage-dependent K^+ channels corresponds to the inner helix of the KcsA K^+ channel, which lines the pore on the intracellular side of the selectivity filter[20]. This region of the pore forms a 10 Å-wide cavity at the membrane centre, the central cavity, that gradually tapers to about 4 Å diameter near the cytoplasmic opening. The pore-lining surface is predominantly hydrophobic in this region of the channel. We mutated amino acids that were predicted to point towards the pore on the basis of the KcsA K^+ channel structure. Five mutations out of six (to alanine) had significant effects on the inactivation gate K_d (Fig. 2c). The effects at positions 551 and 554, corresponding to cavity-lining residues 100 and 103 in KcsA, were so large that the K_d shown is an approximation based on the residual current measured after inactivation (see Methods). We used double-mutant cycle analysis of inactivation gate and inner helix mutations to assess the proximity of amino acids in the inactivated state (Fig. 2d). The Val 3 mutation

* Present address: Department of Molecular Biophysics and Biochemistry, Yale University, 260 Whitney Avenue, New Haven, Connecticut 06520, USA.

on the gate was coupled to the Val 558 and Val 562 mutations on the inner helix, and the Ile 5 mutation was coupled to the Tyr 569 mutation. It was not possible to determine accurately the mutant cycle coupling energies involving positions 551 and 554, but the results at other positions imply that the inactivation gate lies in an extended conformation in the inner pore (Fig. 2d, e).

The central cavity binds hydrophobic cations

The above results support the simple conclusion that the inactivation gate apparently enters the inner pore and lodges its N terminus into the central cavity. To further support this hypothesis, we next made use of the fact that quaternary ammonium inhibitors mimic the action of the inactivation gate[10,11] (Fig. 1a, b). The KcsA K^+ channel was crystallized in the presence of tetrabutylammonium (TBA) and an electron-dense analogue, tetrabutylantimony (TBSb). TBSb is chemically very similar to TBA and blocks K^+ channels accordingly (Fig. 3a). The heavy atom Sb provides the distinct advantage of easy identification in an electron density map. Data were collected from each crystal and a difference electron density map (F_{TBSb}–F_{TBA})PHIcalc was calculated (Fig. 3b; see Methods). The strong electron density peak reveals the binding site for TBA in the cavity. Refinement of the channel–TBA complex indicates that the presence of TBA in the cavity has little influence on the structure. Compared to the structure without TBA, the inner helices are drawn inwards towards the centre by a few tenths of an angstrom at the level of the cavity and are unchanged below the cavity (Protein Data Bank code 1J95).

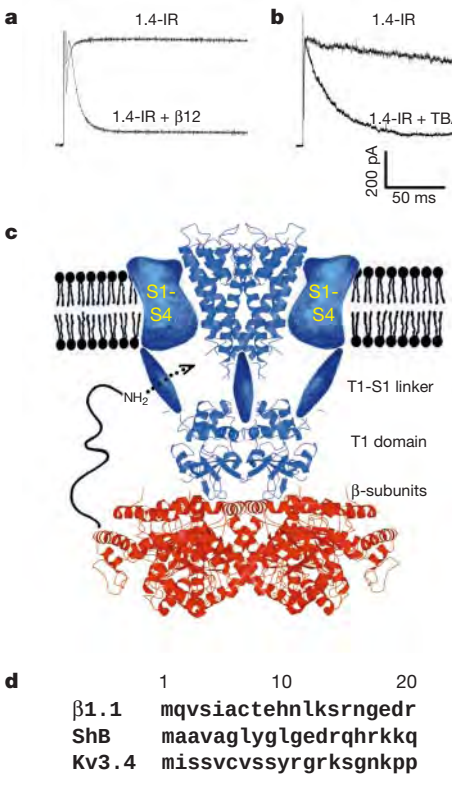

Figure 1 Biophysical features of K^+ channel inactivation. **a**, K^+ currents recorded from *Xenopus laevis* oocytes under two-electrode voltage clamp expressing channels without an inactivation gate (1.4-IR) or with inactivation gates provided by β-subunits (1.4-IR + β12). The maximum current value is 1.4 μA and 2 μA for noninactivating and inactivating currents, respectively. Time scale is given in **b**. **b**, K^+ currents from 1.4-IR channels recorded from an excised, inside-out patch under voltage clamp in the absence (1.4-IR) or presence of 10 μM TBA (+ TBA). **c**, Composite model of a voltage-dependent K^+ channel[16]. The α-subunit is shown in blue and the β-subunit in red. The pore is represented by the KcsA K^+ channel[20] and the T1-β complex is from ref. 16. The structures of the voltage sensor (S1–S4) and linker (T1–S1) connecting the voltage sensors to the T1 domain are unknown. An N-terminal inactivation gate is shown entering a lateral opening to gain access to the pore. The image was prepared by Molscript[30] and raster-3D[31]. **d**, Sequence alignment shows inactivation gates from K_vβ1.1 (accession number CAA 50000), Shaker B (accession number CAA 29917) and K_v3.4 (accession number XP_002146).

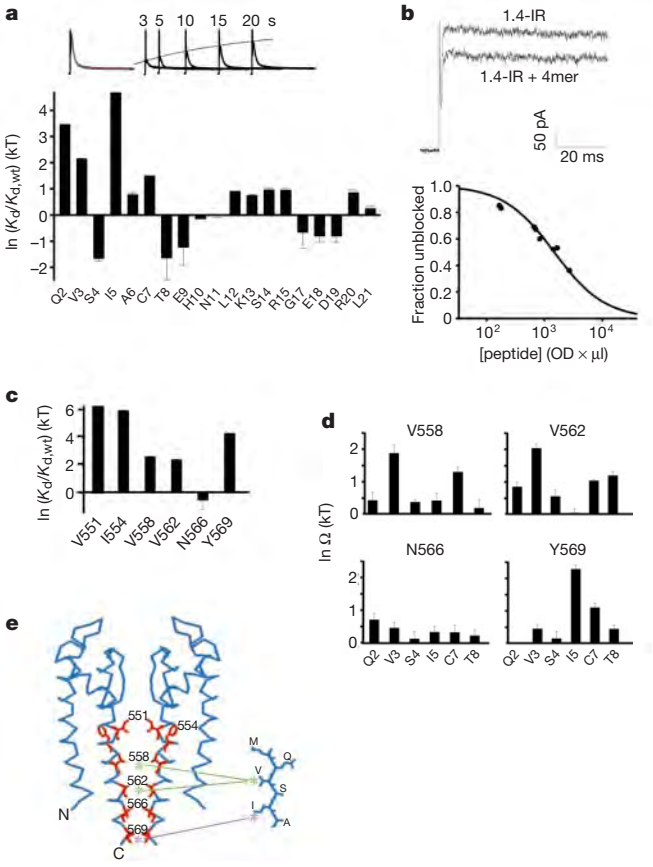

Figure 2 Mutational analysis of the inactivation gate–receptor interaction. **a**, Top, inactivation rates in K_v1.4-IR + β12 channels determined by analysis of currents during a depolarizing pulse from –80 mV to +60 mV and recovery of current during a paired-pulse protocol[7]. τ_{on} (5.0 ± 0.3 ms) is the short time constant of a double exponential fit to current inactivation (red line) and τ_{off} (11 ± 0.7 s) is the time constant describing recovery in paired pulses (black line). Bottom, alanine-scanning mutagenesis of the inactivation gate. K_d, defined as τ_{on}/τ_{off}, was determined for K_v1.4-IR + β12 channels with mutations to alanine or valine (position 6) at positions 2–21 in the β12 inactivation gate. The K_d values, normalized by that for wild type, are shown. Error bars represent s.e.m. from ≥5 oocytes. **b**, Top, current recorded from an excised, inside-out patch containing 1.4-IR channels without (1.4-IR) and with (+ 4mer) a peptide corresponding to the first four amino acids of the β12 inactivation gate. Bottom, dose–response curve showing current inhibition by the 4mer peptide as a function of concentration in units of optical density × volume. Data were collected from 12 patches. **c**, Alanine-scanning mutagenesis of pore-lining residues. The K_d for six pore-lining mutations to alanine, normalized by the wild-type K_d, is shown. Error bars represent s.e.m. from 3–7 oocytes. **d**, Double-mutant cycle analysis between pore-lining residues and residues on the inactivation gate. Ω calculated for six residues on the inactivation gate and four residues on the pore-lining helix is shown. Inactivation did not occur when Y569A on K_v1.4-IR was paired with Q2A on β12. The approximate K_d determination for V551A and I554A mutations did not allow determination of Ω. Error bars show the s.e.m. measured in ≥5 oocytes. **e**, Summary of mutational analysis. Left, two diagonally positioned KcsA K^+ channel subunits are shown in C_α trace, with pore-lining residues of the KcsA K^+ channel shown as sticks but labelled according to K_v1.4 residue numbering. Right, an extended strand model for the first six residues of the inactivation gate with side chains shown as sticks. Green and purple connecting lines identify coupled residues in the mutant cycle analysis.

Inner helix mutations in the 1.4-IR channel alter inactivation and inhibition by TBA in a roughly similar manner (Fig. 3c). This finding further supports a common mechanism in which the inactivation peptide, like TBA, enters the pore and reaches the cavity. One notable difference between the inactivation gate and TBA is evident near the bottom of the inner helix, where the Y569A mutation has a relatively larger effect on inactivation. This difference is reasonable, however, as the inactivation gate comprises 20 amino acids and presumably interacts with the pore all the way from the cavity to the intracellular opening. A comparison of the size of TBA and the inactivation peptide leads us to propose that probably only the first three amino acids of the inactivation peptide bind in the cavity (Fig. 3d). These amino acids are generally hydrophobic in the inactivation gates (the β1 inactivation gate is unusual in having a glutamine in the second position) and contain the N-terminal amino group, and are therefore chemically similar to TBA.

Our data lead us to propose that inactivation occurs through the interaction of the K^+ channel with a fully extended N-terminal peptide. The hydrophobic region of the peptide would extend from the cavity to the intracellular entryway, while the hydrophilic peptide region would emerge from the pore and interact with the aqueous protein surfaces lining the cage formed above the T1 domain (Fig. 1c). This configuration makes good chemical sense as the cavity and inner pore are lined by hydrophobic amino acids and the T1–S1 linkers outside the pore contain many acidic amino acids that would interact favourably with the inactivation peptide's multiple basic residues. This picture is consistent with the deduction of Aldrich *et al.* that the hydrophobic region must be 'buried in a hydrophobic environment' and that the hydrophilic region is important for 'long-range electrostatic interactions'[4,5].

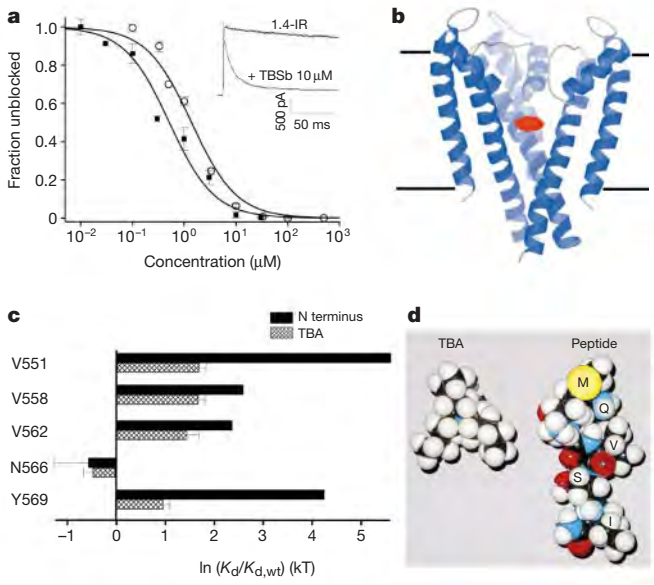

Figure 3 TBA binds in the cavity of the KcsA K^+ channel. **a**, Functional study of TBA and TBSb: currents from excised, inside-out patches were recorded under different TBA (open circles) or TBSb (filled squares) concentrations and fraction of residual current is plotted against inhibitor concentration. Smooth curves correspond to the Langmuir equation with K_d for TBA and TBSb of 1.5 μM and 0.7 μM, respectively. Inset, example currents with and without TBSb (10 μM). **b**, Ribbon diagram of three subunits of the KcsA K^+ channel. The red surface contoured at 6σ is the largest positive peak (maximum 18σ) present in a difference electron density map calculated at 4.0 Å with coefficients F_{TBSB}–F_{TBA} and model phases from a refined model with TBA omitted. **c**, Effects of inner helix (S6) mutations on TBA block and inactivation. For pore-lining mutations on the inner helix, the natural logarithm of K_d for TBA and the inactivation gate (normalized to that of wild type) are plotted. Error bars for inactivation are s.e.m. from 3–7 oocytes. Error bars for TBA block are s.e.m. from ≥5 patches. **d**, CPK models of TBA (left) and the first five residues of the N-terminal inactivation gate (right). The inactivation gate is not at its most extended conformation, but the volume of the first three amino acids is comparable to that of TBA.

Sequential steps of inactivation

The idea that the N-terminal gate snakes into the inner pore as an extended peptide contradicts proposals of a structured inactivation domain docking superficially on the intracellular opening[13,15]. The complex pathway to the intracellular pore opening indicates that the peptide probably reaches its final inactivating configuration through sequential binding steps (Figs 1c, 4a). For example, it is reasonable to imagine that the peptide first binds on the protein surface outside the pore, producing a preinactivated state, and then inserts its hydrophobic region to block the pore as outlined in the kinetic scheme (Fig. 4a):

$$O \underset{k_{-1}}{\overset{k_1}{\rightleftharpoons}} O' \underset{k_{-2}}{\overset{k_2}{\rightleftharpoons}} I$$

The channel would conduct ions in the open (O) and preinactivated (O′) states and become blocked in the inactivated (I) state. The effects of mutations on the forward (onset of inactivation) and backward (recovery from inactivation) rates can offer insight into the relative rates in such a sequential reaction scheme. Here and in previous studies, mutations in the hydrophobic region of the peptide affected mainly the apparent backward rate, I → O, whereas mutations in the hydrophilic region affected modestly both the forward and backward rates[4,5] (Fig. 4b). These observations make perfect sense if k_1 is small and $k_2 \gg k_{-1}$, conditions under which the forward rate O → I will be dominated by k_1 and the backward rate I → O will be related to $k_{-1} \times (k_{-2}/(k_2 + k_{-2}))$. Hydrophobic region mutations, by altering k_2 and k_{-2}, will affect only the backward rate, and hydrophilic region mutations, by altering k_1 and k_{-1}, will affect both rates. We therefore suggest that the first transition to form the

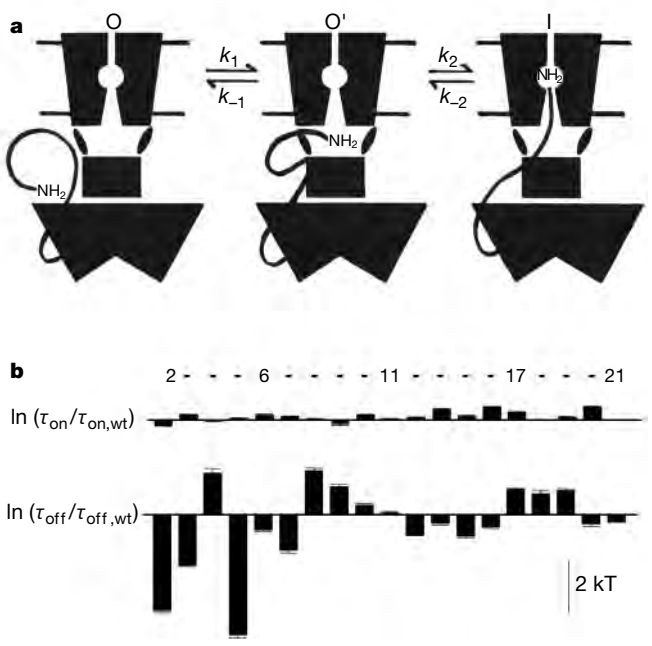

Figure 4 A structural model for the mechanism of inactivation. **a**, Open K^+ channel with three different configurations of the N-terminal inactivation gate shown attached to the β-subunit. For clarity, one inactivation gate is shown instead of four. O, open channel with its N terminus before docking; O′, open channel with its N terminus bound to the hydrophilic protein surface; I, open channel with its N terminus entering the cavity (blocking the channel). **b**, The effect of N-terminal mutations on time constants of inactivation (τ_{on} and τ_{off}). The natural logarithms of inactivation time constants (normalized to that of the wild type) are plotted. Numbers above the bars represent inactivation gate residue numbers (Fig. 2). Error bars are s.e.m. from ≥5 oocytes.

preinactivated state can be rate limiting and that the final plugging transition can be fast, at least in some K^+ channels.

One prediction made by these rate conditions is that the forward rate of inactivation should be nearly voltage independent, as the rate-limiting step occurs outside the membrane electric field. Voltage-independent inactivation is observed in some K^+ channels[6]. A second prediction of these rate conditions is that if a fraction of channels exists in the preinactivated state before opening of the voltage-dependent gate, they should very rapidly inactivate upon opening. If sufficiently rapid, the inactivation peptide would appear to produce closed-state inactivation. Apparent closed-state inactivation has been documented with different inactivation gates of the Shaker splice variants[4]. Moreover, systematic truncation of the Shaker D peptide hydrophilic region modulated the extent of the apparent closed-state inactivation, as the model in Fig. 4a would predict[4].

Discussion

Our findings lead us to conclude that the hydrophobic central cavity and inner pore of K^+ channels form the receptor site for both the inactivation gate and quaternary ammonium compounds. This conclusion explains the following functional properties of inactivation: a single gate is sufficient to cause inactivation[7,8]; quaternary ammonium compounds compete with the inactivation gate[11]; external K^+ pushes quaternary ammonium ions and the gate out of the pore[9,21]; inactivation is voltage independent[6]; and some K^+ channels appear to exhibit closed-state inactivation[4]. A central cavity receptor for molecules as large as TBA and the inactivation gate also has implications for activation gating conformations in K^+ channels. In the KcsA crystal structure, the pore entryway near the cytoplasm has a diameter of about 4 Å. The diameter is unchanged when TBA is present in the cavity, but the pore must open sufficiently wide for TBA or the inactivation gate to reach the cavity.

Many pharmacological agents that influence cation channel function are both hydrophobic and cationic. On the basis of this study, we suggest that many of these agents bind in the cavity[22,23]. □

Methods

Mutagenesis and expression

We used rat K_v1.4-IR (residues 111–655, accession number CAA 34133) and rat β12 chimaera (rat β2 core (residues 36–367, accession number CAA 54142) spliced at the N terminus with rat β1 (residues 1–70, accession number CAA 50000))[16]. We introduced point mutations by the QuickChange method (Stratagene) and confirmed them by sequencing the entire complementary DNA insert. We prepared RNA by T7 polymerase transcription and injected it into *Xenopus laevis* oocytes[24].

Electrophysiology

We used a two-electrode voltage clamp (OC-725B, Warner Instrument Corp.) to record K^+ currents from oocytes 1–2 days after injection with messenger RNA. Electrodes had a resistance of ~0.5 MΩ (3 M KCl). The bath solution contained (in mM): NaCl 96, KCl 2, $CaCl_2$ 0.3, $MgCl_2$ 1 and HEPES 5 at pH 7.4. Oocytes were held at −80 mV and stepped to +60 mV for 200 ms to elicit K^+ current. Data collection and analysis methods are described in ref. 16.

We recorded patch-clamp currents from inside-out, excised patches from oocytes 3–5 days after injection. Electrodes were drawn from patch glass (PG150T-10, Warner Instrument Corp.) and polished to a resistance of 0.6–1 MΩ. The pipette solution (outside) contained (in mM): KCl 140, $MgCl_2$ 2 and HEPES 10 at pH 7.4. The bath solution (inside) contained (in mM): KCl 140, EGTA 5, $MgCl_2$ 2 and HEPES 10 at pH 7.4. K^+ currents were elicited by holding the patch at −100 mV and stepping to +60 mV for 300 ms. Solution exchange was achieved by gravity flow. Analogue data from an Axopatch-1D amplifier (Axon Instruments) were filtered (3 kHz, −3 dB) by an 8-pole Bessel filter (Frequency Devices), digitized at 20 kHz and stored on a PC hard disk.

Synthetic peptide and blockers

Inactivation peptide (4-mer) was synthesized by the Protein/DNA technology Center of the Rockefeller University. Rink amide resin was used to ensure that the C terminus of the peptide was amidated. We purified peptide by reversed-phase high-performance liquid chromatography, dissolved it in bath solution and added it directly to the bath. The peptide amount used was quantified by optical density (at 215 nm) × vol (μl).

We purchased TBA and TBSb from Kodak and Aldrich, respectively. We dissolved TBA or TBSb in bath solution and perfused it onto an inside-out patch by gravity flow.

Crystallography

KcsA was expressed and purified as described[20]. We incubated the chymotrypsin-cut protein at around 10 mg ml^{-1} in a solution containing 150 mM KCl, 50 mM Tris (pH 7.5), 2 mM DTT and 5 mM *N*,*N*-dimethyldodecylamine-*N*-oxide with 1 mM of TBSb or 5 mM TBA for 15–30 min at room temperature. Crystals were obtained as described[20]. Data were collected under a stream of boiled-off nitrogen at stations ID-13, ESRF and X-25, National Synchrotron Light Source, Brookhaven National Laboratory. The TBA co-crystal data extends to 2.8 Å with R_{sym} = 7.2%, 93% complete, redundancy ~2 and the TBSb co-crystal data extends to 3.45 Å with R_{sym} = 7.0%, 97% complete, redundancy ~3. The data were processed with Denzo and Scalepack[25]. All other calculations were done with the CCP4 package[26]. The two data sets were scaled together to 4 Å with R_{merge} = 22.5% before the calculation of the difference electron-density map.

Analysis of inactivation, TBA block and double-mutant cycles

We determined the inactivation gate affinity for the channel by taking the ratio τ_{on}/τ_{off}. This definition approximates the equilibrium constant k_{off}/k_{on} with two sources of error. First, even for a two-state process, $\tau_{on}/\tau_{off} = k_{off}/(k_{on} + k_{off})$. Given that in most channels studied $k_{on} >> k_{off}$, this approximation introduces only a small error. Second, the inactivation process is not a two-state process, as discussed. In a separate analysis we modelled inactivation as a three-step reaction with a slow first and rapid second transition and found that our analysis, assuming two states, was sufficient for parameterization of mutational effects. To determine τ_{on}, we fit the inactivating current with a double exponential function and took the fast component ($\tau < 50$ ms, typically > 90% of inactivation) as τ_{on}. To determine τ_{off}, we fit the envelope of recovery in paired pulse experiments to a single exponential function[7]. In some mutant channels, we had to fit recovery with a double exponential function. We took the faster component ($\tau < 1$ s, 50–80% of current) as τ_{off}. Justification for this assignment is based on previous studies showing that the slow component of recovery is due to C-type inactivation[19,27]. We verified this conclusion in two ways, by raising extracellular K^+ concentration to 96 mM, and by introducing a point mutation (K533Y) at the external TEA binding site[9,28]. Both manoeuvres caused the slow component of recovery to disappear, compatible with its designation as the C-type process. In the case of mutations V551A and I554A, τ_{off} was too small to measure accurately and so we estimated the apparent gate affinity from the fraction of current remaining after inactivation (~87% and ~70%, respectively).

To quantify TBA, TBSb or peptide blocking, we plotted the fraction of residual current at the end of a 300-ms pulse against blocker concentration and fitted it with the following equation to obtain K_d, the equilibrium dissociation constant: fraction unblocked = $1/(1 + [\text{blocker}]/K_d)$.

We used the double-mutant cycle parameter Ω, where

$$\Omega = \frac{K_d^{wt,wt} \times K_d^{mut,mut}}{K_d^{wt,mut} \times K_d^{mut,wt}}$$

to quantify the degree of coupling between two mutants[29]. An Ω value of more than unity indicates that the effects of two mutations are coupled. We used the mean and s.e.m. of K_d to obtain the range of uncertainty on Ω, assuming linear propagation of independent errors through the above equation.

Received 5 March; accepted 19 April 2001.

1. Hoshi,T., Zagotta, W. N. & Aldrich, R. W. Biophysical and molecular mechanisms of Shaker potassium channel inactivation. *Science* **250,** 533–538 (1990).
2. Zagotta, W. N., Hoshi, T. & Aldrich, R. W. Restoration of inactivation in mutants of Shaker potassium channels by a peptide derived from ShB. *Science* **250,** 568–571 (1990).
3. Rettig, J. *et al.* Inactivation properties of voltage-gated K^+ channels altered by presence of β-subunit. *Nature* **369,** 289–294 (1994).
4. Murrell-Langnado, R. D. & Aldrich, R. W. Interactions of amino terminal domains of Shaker K channels with a pore blocking site studied with synthetic peptides. *J. Gen. Physiol.* **102,** 949–975 (1993).
5. Murrell-Langnado, R. D. & Aldrich, R. W. Energetics of *Shaker* K channels block by inactivation peptides. *J. Gen. Physiol.* **102,** 977–1003 (1993).
6. Zagotta, W. N. & Aldrich, R. W. Voltage-dependent gating of Shaker A-type potassium channel in Drosophila muscle. *J. Gen. Physiol.* **95,** 29–60 (1990).
7. MacKinnon, R., Aldrich, R. W. & Lee, A. W. Functional stoichiometry of Shaker potassium channel inactivation. *Science* **262,** 757–759 (1993).
8. Gomez-Lagunas, F. & Armstrong, C. M. Inactivation in ShakerB K^+ channels: a test for the number of inactivating particles on each channel. *Biophys. J.* **68,** 89–95 (1995).
9. Demo, S. D. & Yellen, G. The inactivation gate of the Shaker K^+ channel behaves like an open-channel blocker. *Neuron* **7,** 743–753 (1991).
10. Armstrong, C. M. Interaction of tetraethylammonium ion derivatives with the potassium channels of giant axons. *J. Gen. Physiol.* **58,** 413–437 (1971).
11. Choi, K. L., Aldrich, R. W. & Yellen, G. Tetraethylammonium blockade distinguishes two inactivation mechanisms in voltage-activated K^+ channels. *Proc. Natl Acad. Sci. USA* **88,** 5092–2095 (1991).
12. Isacoff, E. Y., Jan, Y. N. & Jan, L. Y. Putative receptor for the cytoplasmic inactivation gate in the *Shaker* K^+ channel. *Nature* **353,** 86–90 (1991).
13. Antz, C. *et al.* NMR structure of inactivation gates from mammalian voltage-dependent potassium channels. *Nature* **385,** 272–275 (1997).
14. Schott, M. K., Antz, C., Frank, R., Ruppersberg, J. P. & Kalbitzer, H. R. Structure of the inactivating gate from the Shaker voltage gated K^+ channel analyzed by NMR spectroscopy. *Eur. Biophys. J.* **27,** 99–104 (1998).
15. Antz, C. & Fakler, B. Fast inactivation of voltage-gated K^+ channels: From cartoon to structure. *News Physiol. Sci. (Bethesda)* **13,** 177–182 (1998).
16. Gulbis, J. M., Zhou, M., Mann, S. & MacKinnon, R. Structure of the cytoplasmic β subunit-T1 assembly of voltage-dependent K^+ channels. *Science* **289,** 123–127 (2000).

17. Kobertz, W. R., Williams, C. & Miller, C. Hanging gondola structure of the T1 domain in a voltage-gated K^+channel. *Biochemistry* **39,** 10347–10352 (2000).
18. Sokolova, O., Kolmakova-Partensky, L. & Grigorieff, N. Three-dimensional structure of a voltage-gated potassium channel at 2.5 nm resolution. *Structure* **9,** 215–220 (2001).
19. Heinemann, S. H., Rettig, J., Graack, H. R. & Pongs, O. Functional characterization of Kv channel beta-subunits from rat brain. *J. Physiol. (Lond.)* **493,** 625–633 (1996).
20. Doyle, D. A. *et al.* The structure of the potassium channel: molecular basis of K^+ conduction and selectivity. *Science* **280,** 69–77 (1998).
21. Armstrong, C. M. & Hille, B. The inner quaternary ammonium ion receptor in potassium channels of the node of Ranvier. *J. Gen. Physiol.* **59,** 388–400 (1972).
22. Yarov-Yarovoy, V. *et al.* Molecular determinants of voltage-dependent gating and binding of pore-blocking drugs in transmembrane segment IIIS6 of the Na^+ channel alpha subunit. *J. Biol. Chem.* **276,** 20–27 (2001).
23. Mitcheson, J. S., Chen, J., Lin, M., Culberson, C. & Sanguinetti, M. C. A structural basis for drug-induced long QT syndrome. *Proc. Natl Acad. Sci. USA* **97,** 12329–12333 (2000).
24. Lu, Z. & MacKinnon, R. A conductance maximum observed in an inward-rectifier potassium channel. *J. Gen. Physiol.* **104,** 477–486 (1994).
25. Otwinowski, Z. in *Proceedings of the CCP4 Study Weekend* (SERC Daresbury Laboratory, Daresbury, UK, 1993).
26. Collaborative Computational Project Number 4. The CCP4 suite: programs for protein crystallography. *Acta Crystallogr. D* **50,** 760–763 (1994).
27. Rasmusson, R. L. *et al.* C-type inactivation controls recovery in a fast inactivation cardiac K^+channel (Kv1.4) expressed in *Xenopus* oocytes. *J. Physiol. (Lond.)* **489,** 709–721 (1995).
28. MacKinnon, R. & Yellen, G. Mutations affecting TEA blockade and ion permeation in voltage-activated K^+ channels. *Science* **250,** 276–279 (1990).
29. Hidalgo, P. & MacKinnon, R. Revealing the architecture of a K^+ channel pore through mutant cycles with a peptide inhibitor. *Science* **268,** 307–310 (1995).
30. Kraulis, P. MOLSCRIPT: a program to produce both detailed and schematic plots of protein structures. *J. Appl. Crystallogr.* **24,** 946–950 (1991).
31. Merritt, E. A. & Bacon, D. J. Raster3D: Photorealistic molecular gaphics. *Methods Enzymol.* **277,** 505–524 (1997).

Acknowledgements

We acknowledge the European Synchrotron Radiation Facility (ESRF) and the National Synchrotron Light Source (NSLS) at Brookhaven National Laboratory (with support by the U.S. D.O.E., Division of Material Sciences and Division of Chemical Sciences). We thank C. Petosa and A. Perrakis for help on ESRF ID-13, and M. Becker for help on NSLS X-25. The project was supported by an NIH grant to R.M. R.M. is an investigator in the Howard Hughes Medical Institute.

Correspondence and requests for materials should be addressed to R.M. (e-mail: mackinn@rockvax.rockefeller.edu). Coordinates have been deposited with the Protein Data Bank under accession code 1J95.